Effective elastin-like recombinamers coating on poly(vinylidene) fluoride membranes for mesenchymal stem cell culture

Maria Guillot-Ferriols [a,b] *, Ana del Barrio [c], Carlos M. Costa [d,e],

Senentxu Lanceros Méndez [d,f,g], José Carlos Rodríguez-Cabello [b,c],

José Luis Gómez Ribelles [a,b], Mercedes Santos [b,c], Gloria Gallego Ferrer [a,b]

[a] *Centre for Biomaterials and Tissue Engineering (CBIT), Universitat Politècnica de València, 46022 Valencia, Spain*
[b] *Biomedical Research Networking Center on Bioengineering, Biomaterials and Nanomedicine (CIBER-BBN), Valencia, Spain*
[c] *BIOFORGE Group, Centro de Investigación Científica y Desarrollo Tecnológico, Universidad de Valladolid, 47011, Valladolid, Spain*
[d] *Centre of Physics, Universidade Do Minho, 4710-058 Braga, Portugal*
[e] *Centre of Chemistry, Universidade Do Minho, 4710-058 Braga, Portugal*
[f] *BCMaterials, Basque Center for Materials, Applications and Nanostructures, UPV/EHU Science Park, 48940 Leioa, Spain*
[g] *IKERBASQUE, Basque Foundation for Science, 48013 Bilbao, Spain.*

ABSTRACT

Bone's inherent piezoelectricity is a key factor in regulating bone growth and mesenchymal stem cells (MSCs) fate towards the osteogenic lineage. The piezoelectric polymer poly(vinylidene) fluoride (PVDF) was thus used to manufacture electroactive membranes by means of non-solvent induced phase separation (NIPS), producing porous membranes with approximately 90 % of γ-phase for MSCs culture. The combination of the porous surface and PVDF hydrophobicity hinders cell adhesion and requires a coating to improve cell culture conditions. A layer-by-layer (LbL) method was used to deposit elastin-like recombinamers (ELRs) containing RGD sequences

applying click cross-linking chemistry. ELRs potential was confirmed by comparing traditional fibronectin adsorption with ELRs LbL on PVDF electroactive membranes. Porcine bone marrow MSCs preferred ELRs-coated surfaces, which enhanced initial cell adhesion and improved proliferation after 7 days. These findings lead to new possibilities for regenerative therapies in the area of bone tissue engineering, offering the advantages of MSC commitment towards the osteogenic lineage by applying electro-mechanical stimulation on electroactive substrates.

KEYWORDS: Poly(vinylidene) fluoride; piezoelectricity; elastin-like recombinamers; RGD; layer-by-layer; mesenchymal stem cells

1. INTRODUCTION

Poly(vinylidene) fluoride (PVDF) is a piezoelectric semi-crystalline polymer which can crystallize into five polymorphs, α, β, γ, δ and ε. Chain conformations, all trans (TTT) planar zigzag and T_3GT_3G for β and γ phases respectively [1], and the electronegativity difference between fluorine and hydrogen atoms create a net dipole moment in these polymorphs and confer them electroactive properties [2].

PVDF has been proposed as a candidate for bone tissue engineering (TE) applications due to its capacity to produce a surface charge variation when a mechanical input is applied [3], reproducing bone's inherent piezoelectricity, as discovered by Fukada and Yasuda [4]. This mechanism is hypothesized to be involved in bone's capacity to adapt to mechanical stress and tissue regeneration [5]. Electro-mechanical stimulation has been shown to enhance cell viability, proliferation and differentiation on osteogenic progenitors [6–8].

Specific bioreactors, compatible with cell culture conditions, have been designed to fulfil the need of transmitting stimulus or cues to different cell types cultured on a wide variety of supports [9,10]. As a matter of fact, bioreactor systems based on a vertical vibration module have been used to electro-mechanically stimulate human adipose stem cells, mechanically deforming the PVDF matrix and transmitting the electrical stimulus to the cells [11,12].

The interest in using PVDF in bone TE lies in the presence of the electroactive phases, which can be obtained during the manufacturing process. The PVDF α-phase is usually obtained as crystallization from the melt results in this polymorph [13]. The β-phase can be produced by uniaxial stretching of the α polymorph [14], which is a two-step process. Crystallization below 70 ºC using polar solvents such as dimethylformamide can obtain both β and γ electroactive phases [15,16], reducing the manufacturing process to a single step [17] and allowing the support to be manufactured in complex shapes.

Non-solvent induced phase separation (NIPS), which consists of the precipitation of the polymer cast on a surface by immersing it in a coagulation bath containing a non-solvent, is compatible with the above-mentioned parameters [18,19]. Different topographies and diverse electroactive contents can be obtained from different applied manufacturing conditions [20] in a reliable, cost-effective and simple method of producing electroactive PVDF supports for cell culture [21].

When considering PVDF for biological applications the surface properties must be modified to control cell behaviour due to its high hydrophobicity [22]. When culturing cells with osteogenic characteristics fibronectin adsorption is usually applied to enhance their initial adhesion and proliferation [8,11,23], however fibronectin has proven to be ineffective in highly porous PVDF supports regarding mesenchymal stem cell (MSCs) adhesion [24].

Elastin-like recombinamers (ELRs) have arisen as suitable biomolecules for biomimetic polymer coatings that include specific biofunctional sequences. ELRs are synthetic elastin-inspired polypeptides, produced by DNA recombinant technologies, formed by repetitive sequences comprising the most widely used pentapeptide domain Val-Pro-Gly-X-Gly (VPGXG), X being any natural or modified amino acid, with the exception of L-proline [25]. ELRs can be engineered to incorporate bioactive sequences with specific properties for cell attachment, proliferation and differentiation [26]. In this regard, the Arg-Gly-Asp (RGD) sequence, found in a number of extracellular matrix proteins, is known to mediate cell attachment and spreading [27,28]. This domain was one of the first bioactive motifs introduced to the ELR main chain [29] and was applied as a substrate coating, showing improved cell affinity [30]. Besides mediating cell adhesion, the RGD sequence has been shown to be involved in MSCs differentiation towards the osteogenic lineage [31–34].

Biocompatible ELRs click hydrogels can be obtained by interchain crosslinking via catalyst-free Hüisgen 1,3-dipolar cycloaddition under physiological conditions in a mild and cell-friendly process with atom economy[35]. These click hydrogels are outstanding candidates for tissue engineering [36] in general and as layer-by-layer (LbL) stable and biomimetic coatings, with increased adhesion and proliferation when RGD is incorporated, establishing the basis of future biomedical applications [37].

In this study we combined electroactive PVDF membranes produced by NIPS with ELRs containing RGD sequences deposited on their surface by the LbL technique, applying the click crosslinking approach, as cell culture supports for *in vitro* mesenchymal stem cell culture. The effectiveness of ELRs LbL coating on PVDF electroactive supports was compared with traditional fibronectin adsorption using porcine bone marrow MSCs. The results on cell proliferation on the

ELRs-coated materials obtained show that they are promising candidates for electro-mechanical stimulation approaches.

2. MATERIALS AND METHODS

2.1 Electroactive membrane preparation

Poly(vinylidene) fluoride membranes were produced by the non-solvent induced phase separation technique, for which a 20 % w/v PVDF solution (Solef® 6010 PVDF Homopolymer, Solvay) was prepared in dimethylformamide (DMF) (Scharlab, synthesis grade). The solution was magnetically stirred at 60 ºC until complete dissolution of the polymer. Prior to membrane preparation, the solution was kept non-stirred for 30 min to remove air bubbles and then spread on a glass plate with a 750 μm casting knife. The plate was immersed in a coagulation bath containing absolute ethanol (Scharlab) at 25 ºC for 1 h. After complete precipitation, the membranes were washed under agitation for 24 h in deionized water to remove excess ethanol and remaining traces of DMF, with a water change every two hours. Once washed, the membranes were frozen at -80 ºC and lyophilized for 24 h.

2.2 Membrane characterization

2.2.1 Morphological analysis

Membrane surface and cross-section morphology were analysed by means of Field Emission Scanning Electron Microscopy (FESEM). Samples were coated with platinum following a standard sputtering protocol for 90 s (JFC 1100, JEOL, Japan) and visualized in an Ultra 55 microscope (Zeiss). Accelerating voltage was 2 kV. Surface spherulite diameter was measured using ImageJ software (National Institutes of Health, Bethesda, Maryland, USA). Three different membranes from three different batches were analysed with 100 spherulites per sample.

ELRs deposition by the layer-by-layer technique was also confirmed by acquiring images of the coated surface and the cross-section by FESEM applying an accelerating voltage of 1 kV.

Porosity of the developed membranes was measured filling the pores with ethanol and applying Eqs. (1) and (2):

$$V_{pores} = \frac{m_{wet} - m_{dry}}{\rho_{ethanol}} \quad (1)$$

$$\emptyset = \frac{V_{pores}}{V_{pores} + V_{PVDF}} \quad (2)$$

where m_{wet} and m_{dry} are the weight of the membranes before and after immersion in ethanol, respectively. $\rho_{ethanol}$ is ethanol density (0.789 g/cm^3). PVDF volume (V_{PVDF}) was calculated from the dry weight of the membrane and assuming a density of 1.775 g/cm^3.

Three replicates per sample were measured from three different samples produced in different preparations.

2.2.2 Analysis of the electroactive phases

The electroactive phase content present in the membranes was assessed by Fourier-transform Infrared Spectroscopy (FTIR-ATR). Benz and Euler [38] defined a simple method to quantify PVDF crystalline phases present in a sample, especially in the remarkable presence of γ-phase. Different phases were identified by their representative absorption bands (762 cm^{-1} for α, 1279 cm^{-1} for β and 835 cm^{-1} for γ). Since the absorption band at 835 cm^{-1} has contributions from β, γ

and the amorphous phase, the γ -phase fraction (F(γ)) present in the sample can be calculated applying the following equations [38,39]:

(3) $$F(\gamma) = \frac{X_\gamma}{X_\gamma + X_\alpha}$$

(4) $$A_{835} = (K_\gamma^{835} X_\gamma + K_\beta^{835} X_\beta + K_{am}^{835}(1 - X_{total}))t$$

(5) $$A_{762} = K_\alpha^{762} X_\alpha t$$

(6) $$A_{1279} = K_\beta^{1279} X_\beta t$$

Where X_α and X_γ are the fraction of α and γ phases and A_α and A_γ are their absorptions at 762 and 835 cm^{-1}, respectively. K is the characteristic absorption coefficient at the characteristic wavenumber of each of the phases (K_α^{762} = 0.365 μm^{-1}, K_γ^{835} = 0.15 μm^{-1}, K_{am}^{835} = 0.0259 μm^{-1} [38]), X_{total} is total sample crystallinity and *t* is its thickness. The β-phase contribution to Eq. (4) is negligible since there is no peak presence at 1279 cm^{-1}. Also, the high crystallinity of the membranes makes $K_\gamma^{835} X_\gamma$ much larger than $K_{am}^{835}(1 - X_{total})$ and K_γ^{835} is five times larger than K_{am}^{835}. In this case, Eq. (3) can be reduced to:

$$F(\gamma) = \frac{A_{835}}{\left(\frac{K_{\gamma}^{835}}{K_{\alpha}^{762}}\right) A_{762} + A_{835}} \quad (7)$$

Measurements were taken on an ALPHA FTIR spectrometer (Bruker) in ATR mode from 4000 to 400 cm^{-1} at a wavelength resolution of 4 cm^{-1}. Three different membranes from three different batches were analysed.

2.2.3 Membrane's crystalline content

Differential Scanning Calorimetry was used to determine the degree of crystallinity (X_c) of the PVDF membranes produced and their melting temperature. The samples were scanned in a DSC Pyris 1 (PerkinElmer) calorimeter, previously encapsulated in aluminium pans, from 0 °C to 200 °C at a heating range of 20 °C/min in a dry nitrogen atmosphere.

X_c was determined by means of the following equation [38–40]:

$$X_c = \frac{\Delta H_m}{\Delta H_{100}} \times 100 \quad (8)$$

Where ΔH_m is the melting enthalpy of the PVDF membranes measured in DSC and ΔH_{100} is the melting enthalpy for a 100 % crystalline sample of pure PVDF, whose value is 104.7 J/g [41]. Three different membranes from three different batches were analysed.

2.2.4 Poling method and piezoelectric coefficient evaluation

The porous membranes were poled by the contact method, with the polymer membranes placed inside a silicone oil bath to prevent electrical breakdown. Adhesive aluminium tape was used as electrode materials on both membrane surfaces. Polarization conditions were optimized to a final electric field of ~10 kV at a constant current of 10 μA for 1 h at a temperature of 120 ºC.

After the poling time, the membranes were cooled down to room temperature under the application of the electric field.

The piezoelectric d_{33} response was analysed on a Wide Range d33-meter (Model 8000, APC Int Ltd).

2.3 ELRs deposition on PVDF membranes

2.3.1 Biosynthesis and purification of ELRs

ELRs were bioproduced by genetic engineering technology and purified by Inverse Transition Cycling (ITC) [42,43], exploiting their thermosensitive behaviour. The ELR thus obtained was named as HRGD and its amino acid sequence was:

HRGD: MGSSHHHHHHSSGLVPRGSH-MESLLP-{[(VPGIG)2(VPGKG)(VPGIG)2]2-AVTGRGDSPASS- [(VPGIG)2(VPGKG)(VPGIG)2]2]}6-V

The polymer contained VPGKG pentapeptide located uniformly along the main chain to enable further chemical modification through the ε-amine group of lysines. The HRGD biopolymer also contained the peptide loop found in human fibronectin, the carrier of the specific RGD sequence for cell adhesion. ELR purity and chemical characterization were verified by sodium dodecyl sulphate polyacrylamide gel electrophoresis (SDS–PAGE), matrix-assisted laser desorption/ionization time-of-flight (MALDI-ToF) mass spectrometry, amino acid composition

analysis, differential scanning calorimetry (DSC) and nuclear magnetic resonance (NMR) [44]. ^{1}H-NMR spectroscopy and MALDI-ToF-mass spectrometry were carried out in the Instrumental Techniques Laboratory (LTI) of the Research Facilities of the University of Valladolid.

2.3.2 ELRs chemical modification

ELRs were chemically modified to carry cyclooctyne or azide groups in the lateral chain, obtaining the corresponding modified biopolymers (the one bearing cyclooctyne derivatization was labelled RGD-CO and the one with azide groups RGD-N3). The biopolymer chemical functionalization was carried out by modifying the ε-amine groups, as previously described [35].

To modify HRGD with a cyclooctyne group, the ELR was dissolved in DMF (Sigma) at a final concentration of 0.05 g/mL at room temperature in an inert atmosphere. Bicyclo [6.1.0] non-4-yn-9-yl-methyl N-succinimidyl carbonate (0.6 eq, Mw 291.30 mg/mmol, GalChimia, A Coruña, Spain) dissolved in DMF was then added to the ELR solution at a final concentration of 3.3 mg/mL. The resulting mixture was stirred for 48 h at room temperature in an argon atmosphere. The modified RGD-CO was purified by precipitation with diethyl ether. The resulting white solid was washed 3 times with acetone and dried under reduced pressure. The solid was re-dissolved in cold ultrapure MQ water at 4 °C, dialyzed against MQ water, filtered through 0.22 μm filters (Nalgene) and the sterile solution was freeze-dried prior to storage.

Following the same procedure, HRGD was modified to bear an azide group. This time 2-Azido ethyl (2,5-dioxopyrrolidin-1-yl) carbonate (0.6 eq, Mw 228.17 mg/mmol, GalChimia, A Coruña, Spain) was dissolved in DMF and then added to the ELR solution at a final concentration of 1.3 mg/mL. RGD-N3 was purified as previously described.

The modified RGD-CO and RGD-N3 biopolymers were characterized by NMR, MALDI-ToF and Fourier-transform infrared spectroscopy (FTIR-ATR) (supplementary material). MALDI-ToF and ^{1}H-NMR (in DMSO-d6) enabled us to quantify the degree of lysine modification.

2.3.3 Layer-by-Layer procedure for ELRs-covered PVDF membranes

PVDF membranes cut into 1 cm^2 squares were used as the substrate for the ELRs coating. The square surfaces were indicated by a sign on the opposite face to the cell culture. These substrates were first cleaned and activated by argon plasma treatment. This treatment is a cleaning and activation step aimed at promoting a better coating improving adsorption of the first layer onto the surface. The membranes were placed in the chamber and vacuum was generated (P=600 mTorr), a high-frequency (29.6 W) 20 mL/min argon plasma flow passed through the samples for the appropriate time (1, 5, 20 and 30 minutes) to optimize the plasma treatment activation time.

Secondly, different ELRs solution concentrations and immersion orders were studied to achieve the best coating for cellular assays. The ELRs modified with either cyclooctyne or azide groups were dissolved at 10 or 25 mg/mL, according to the assay, in water at 4 ºC overnight and stored at this temperature in separate containers. pH value of the different solutions was 7.5. pH control is less critical than in other conventional layer-by-layer protocols since the link between layers is produced by click reaction between azide and cyclooctine groups, non-acid species. Selecting the optimized plasma treatment protocol, the activated PVDF membranes were sequentially immersed in the ELRs solutions with either RGD-N3 or RGD-CO as the first layer for two seconds and left to dry for five minutes between dippings to generate the first bilayer. A drying step, instead of washing, was chosen in order to assure that the click reaction between the layers was produced. Washings would probably remove the coating without letting the covalent crosslink to end. The

process was then repeated and after being left to dry for 45 minutes the membranes were freeze-dried. Two bilayers were selected as the optimal number of layers as it was enough to completely cover the surface obtaining the thinnest membrane coating.

The optimized protocol is described in Scheme 1.

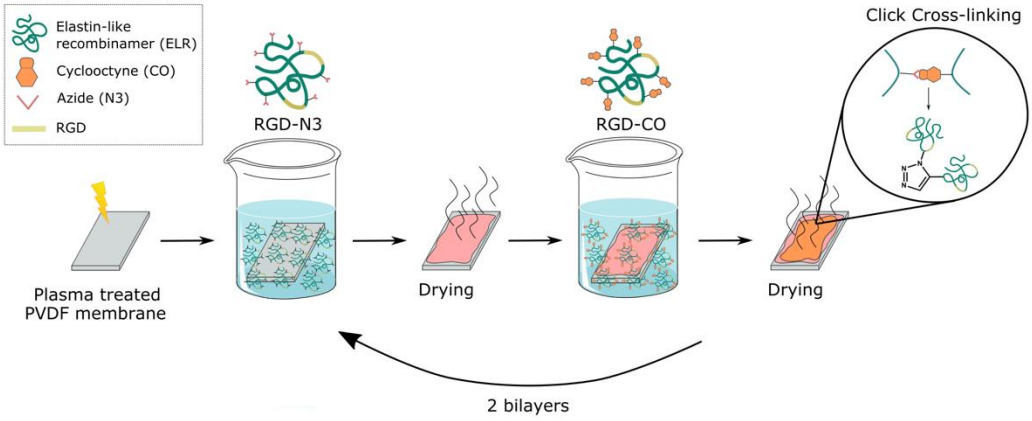

Scheme 1. *Illustration of the optimized layer-by-layer process with RGD-N3 (as first layer) and RGD-CO ELRs onto plasma treated PVDF membranes.*

2.3.4 Characterization of ELRs-covered PVDF membranes

As process control, the non-activated, activated and the final biofunctionalized membranes were evaluated by contact angle measurements determined by a sessile drop method using a Data Physics OCA20 instrument equipped with an adapted CCD video camera. The coating performance was analysed by Fourier-transform infrared spectroscopy (FTIR-ATR) on a Bruker TENSOR 27 acquiring 64 scans between 500-4000 cm^{-1} to compare the spectra of the biofunctionalized, plasma treated and non-coated membranes. The membrane surfaces and cross-section morphology were analysed by FESEM as described in Section 2.2.1.

2.4 Cell culture assays

Porcine bone marrow mesenchymal stem cells (pMSCs) were used to study the cell proliferation response. pMSCs were expanded in basal medium containing Dulbecco's modified Eagles medium (DMEM) high glucose (4.5 g/L) with GlutaMAX^{TM} (Gibco), 10 % (v/v) Foetal Bovine Serum, FBS (Gibco), 100 U/mL penicillin-100 μg/mL streptomycin, P/S (Life technologies), and 5 ng/mL of Fibroblast Growth Factor 2, FGF-2 (Eurobio), at 37 ºC in a humidified atmosphere with 5 % CO_2. All the experiments were performed in passage 5.

After choosing the best layer-by-layer protocol for ELRs deposition, coated (PVDF + ELRs) and non-coated membranes (PVDF) were cut into 8 mm disks to fit on the bottom of a 48 well plate. Samples were sterilized by UV for 20 minutes on each side, after which the membranes were washed in ethanol 70 % (v/v) for 15 minutes under shacking and washed 6 times in Dulbecco's Phosphate Buffered Saline, DPBS (Sigma-Aldrich) to eliminate possible traces of ethanol.

Glass slides, used as controls, were sterilized by sonication in ethanol for 10 minutes and then were exposed to UV for 20 minutes each side.

After sterilization, the non-coated membranes and glass slides were incubated in a solution of human plasma fibronectin (Sigma-Aldrich; 20 μg/mL) for 1 hour at room temperature. Fibronectin coating was used to compare the effectiveness of ELRs layer-by-layer deposition and the traditional protein adsorption. After fibronectin coating, the samples were washed twice with DPBS to remove non-adsorbed fibronectin.

The samples were placed in a 48 well plate, 3 replicates per group, and silicon rings were used to prevent the membranes from floating inside the wells, glass slides included. Basal medium without FBS or FGF-2 was added to the wells to condition the membranes before cell seeding.

12 h before cell seeding, the cells were starved in basal medium containing 1 % (v/v) FBS to synchronize the cell cycle. To study cell proliferation the cells were seeded at a density of 8 x 10^3 cells/cm^2 in basal medium without FBS to promote cell adhesion either to fibronectin or ELRs containing RGD sequences. 100 μL containing the required number of cells was deposited on top of each sample inside the silicon rings. 3 h later, after cell attachment, the required volume of basal medium and FBS for a final concentration of 10 % (v/v) was added to each well.

The medium was changed every 2 or 3 days. After 24 h, 3 and 7 days the samples were fixed in a 4 % (v/v) paraformaldehyde solution (Panreac) for 20 minutes.

Initial adhesion and proliferation studies were carried out by means of staining cell cytoskeleton and nucleus. After fixation, the samples were permeabilized and blocked in 1 % (w/v) bovine serum albumin (BSA; Sigma-Aldrich) solution in DPBS/0.1 % (v/v) Tween-20 (Sigma-Aldrich) for 1 h at room temperature and then incubated with Alexa Fluor Phalloidin 488 (1:100 Fisher Scientific) for 2 hours in a humidified chamber. After washing the samples 3 times with DPBS/0.1 % (v/v) Tween-20 (Sigma-Aldrich), the PVDF membranes were treated with Sudan Black B solution following the protocol described in Morales-Román et al. [24]. As PVDF autofluorescence hinders image acquisition and cell counting, Sudan Black B treatment is necessary to obtain quality images of the cells. The samples were then washed 3 times with DPBS and incubated for 20 minutes with DAPI (1:200; Sigma-Aldrich) in mounting medium.

Four representative areas of each sample were studied, acquiring images with a fluorescence microscope (Nikon Eclipse 80i). The images were analysed on ImageJ software (National Institutes of Health, Bethesda, Maryland, USA). Two independent assays were carried out with three replicates per group. Results were normalized by initial cell seeding density (8 x 10^3 cells/cm^2) and calculated as relative cell proliferation, expressed as Log_2 of the ratio obtained. Each unit represents a doubling in the cell population. This representation method highlights MSCs initial adhesion and proliferation rate on the different conditions tested. Negative values indicate that the number of retained cells is lower than the initial number of seeded cells onto the biomaterial.

2.5 Statistical analysis

All results were expressed as mean ± standard deviation. Statistical analysis was performed on SPSS Software. Two-way ANOVA analysis was applied to the homogeneous groups after checking homoscedasticity by the Levene test. A 95 % confidence interval was set to accept significant inter-group differences (*p-value* < 0.05).

3. RESULTS AND DISCUSSION

3.1 Membrane characterization

PVDF membranes were produced by non-solvent induced phase separation (NIPS) in an ethanol bath at 25 ºC. Of the wide variety of parameters, the selection of the proper non-solvent in the coagulation bath is instrumental in membrane morphology formation. As PVDF is a semi-crystalline polymer, its precipitation during this process is determined by two events associated with crystallization: liquid-liquid demixing and solid-liquid demixing [20]. The presence of

ethanol in the coagulation bath, a soft non-solvent, reduces the solvent-nonsolvent exchange, allowing crystallization, a slower process, before liquid-liquid demixing takes place. Membrane structure and morphology were characterized by FESEM, as shown in Figure 1. Figure 1 (b) shows the symmetrical PVDF membranes with both porous surfaces on the top (Figure 1 (a)) and bottom (images of the bottom surface are not displayed). The use of soft solvents in the coagulation bath gives rise to symmetric membranes without the characteristic presence of finger-like structures or macrovoids present in water-bath produced membranes [45]. Crystallization occurs before crossing the binodal line, allowing crystalline globules to grow and coalesce [15].

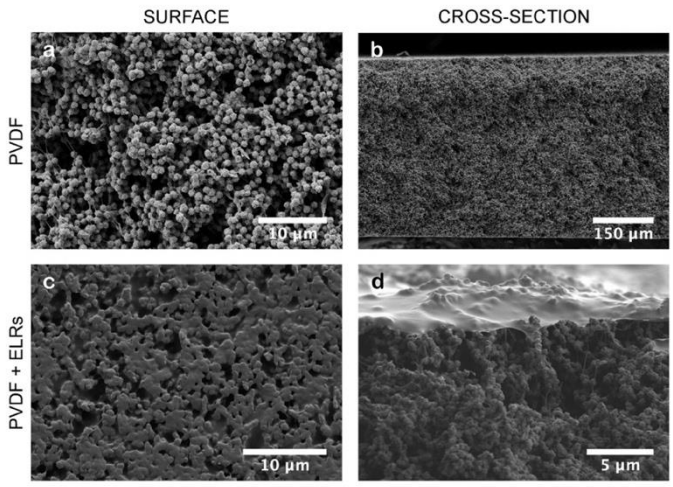

Figure 1. *Surface and cross-section FESEM images of PVDF membranes produced by non-solvent induced phase separation before ELRs deposition by layer-by-layer (a and b) and after (c and d).*

Surface topography is formed by a particulate-like morphology composed of PVDF globules or microbeads. These structures measure 1.1 ± 0.2 µm, in agreement with previous results reported by Lin et al [46]. Pagliero et al. [15] manufactured PVDF membranes in ethanol baths varying the PVDF concentration in the initial solution. Highly concentrated PVDF solutions (above 14 % w/v) gave rise to smaller spherulites than the ones obtained from diluted solutions. A polymer

concentration rise in the initial solution increases solution viscosity, favouring PVDF entanglements, restraining chain mobility and reducing spherulite growth, generating a more compact interconnected network, as in the case of the present membranes using 20 % w/v PVDF solution as shown in Figure 1 (a). These globules are connected to each other by fibrils, probably with the thickness of one or more folded lamellae, as previously reported by Lin et al.[47].

Porosity was determined by filling the membrane pores with ethanol and applying Eqs. (1) and (2). Ethanol was chosen since PVDF is hydrophobic and its pores cannot be filled with water and this would underestimate the pore volume [24]. The PVDF membranes produced by NIPS in an ethanol coagulation bath had a porosity of 81.7 ± 0.5 %.

Fourier-transform infrared spectroscopy (FTIR) has proven to be a valid method of identifying and quantifying the PVDF polymorphs present in different samples, applying the equations cited in Section 2.2.3. Martins et al. [2]reviewed the characteristic absorption bands of the most common crystalline phases α, β and γ. The non-electroactive α-phase is defined by the wavenumbers at 532, 614, 762, 795, 855, 976 cm^{-1}, the most representative and thus used to calculate its fraction being at 762 cm^{-1}. The bands at 445, 510, 840 and 1279 cm^{-1} are used to identify the β-phase, while 431, 512, 812, 835 and 1234 cm^{-1} are used for the γ-phase.

The representative FTIR-ATR spectrum of PVDF membranes is displayed in Figure 2 (a). α-phase characteristic bands at 614, 762 and 976 cm^{-1} can be seen, as highlighted in the graph. Surprisingly, no β-phase peaks are present, especially the absence of one at 1279 cm^{-1}. However, most of the γ-phase characteristic bands can be found in the sample, including 431, 835 and 1234 cm^{-1}. Since 1234 cm^{-1} tends to appear as a shoulder, 835 cm^{-1} is used to quantify the percentage of γ-phase present in the membranes [38–40,48]. The absence of β-phase peaks makes its contribution to this

835 cm^{-1} negligible, allowing Eq. (7) to be applied to obtain the γ-phase fraction. The γ-phase is 93.3 ± 1.4 %, with just a small contribution from the α-phase (6.7 ± 1.4 %).

Using FTIR to identify electroactive β and γ phases is still a subject of debate, since their similar structure provides characteristic absorption bands which are a superposition of both phases. Traditionally, the band at 840 cm^{-1} has been used to identify the β-phase. Nonetheless, the presence of this band is sometimes shown as a shoulder at 833 cm^{-1} in the 840 cm^{-1} band, or as it is the case in the spectrum presented, the peak appears displaced towards 835 cm^{-1} indicating the presence of the γ-phase. This subtle displacement alone is not enough to assure the presence of this polymorph, however bands at 1279 and 1234 cm^{-1} can be used to clearly identify them, since the β and γ contributions, respectively, are unique at these wavenumbers.

Obtaining the γ-phase is more difficult than β and traditionally has only been achieved by isothermal crystallization at extremely high temperatures and slow cooling rates [49]. Adding fillers [40] and crystallization under vacuum [50] have also produced PVDF supports in this electroactive phase. Some authors have reported obtaining it by means of NIPS [16,39]. Highly polar solvents, such as dimethylformamide or dimethylacetamide, favour crystallization in trans phases due to their interaction with the polymer, rotating the C-F bond around the C-C bonds of the chain backbone [51]. In other words, the membranes' γ-phase is produced by the dipole rotation (α to γ) induced by solvent polarity. The presence of alcohols in the coagulation bath has been found to favour the interaction between its -OH groups and the DMF solvent [39]. This phenomenon partially allows the rotation back to α conformation, leading to the low contribution to the sample content.

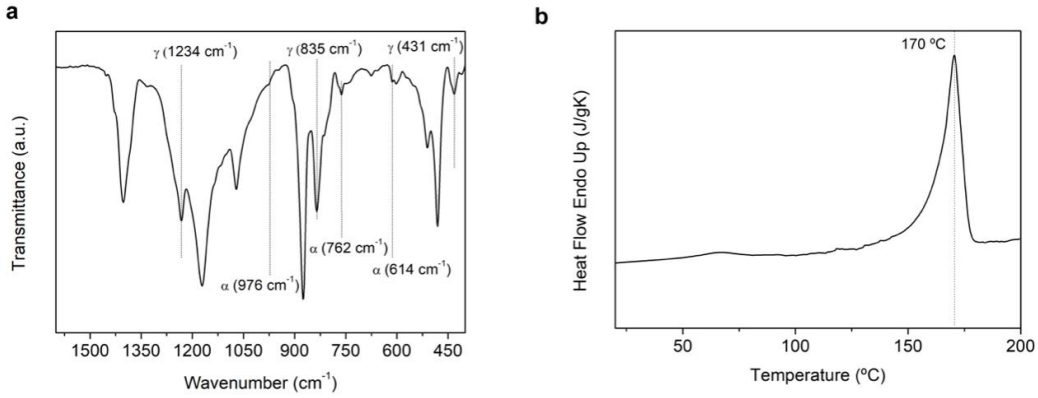

Figure 2. *Representative (a) FTIR-ATR spectrum and (b) DSC curve of PVDF membranes produced by non-solvent induced phase separation.*

Membrane electroactive potential was confirmed by measuring the piezoelectric d_{33} response after poling the samples. Corona discharge poling could not be used due to the high membrane porosity (up to 80 %), which produced an electrical breakdown, so the direct contact poling method filling the pores with silicone oil was used. Immediately after polarization, the $|d_{33}|$ response (typical negative values for PVDF were obtained) varied between 3 and 6 pC/N, depending on the position of the measurement site.

The obtained d_{33} coefficient is in agreement with the values expected for γ-phase PVDF, - 7 pC/N as reported by Lopes et al. [40] for PVDF samples containing 91 % of γ-phase, confirming the majority presence of this polymorph in the produced membranes.

These piezoelectric membranes were coupled to a readout electronic circuit [52] to determine the voltage generated under cycling pressure solicitation by gentle finger pressing and releasing. The output of the amplifying circuit in unloaded conditions, as shown by Gonçalves et al. in [52], averaged to 2.5 V, leading to non-zero voltage values when the membrane was not pressed. When loading was applied by finger pressing, a negative voltage peak was generated while a positive

peak appeared when released. Figure 3 shows the voltage generated when the membrane was under cycling pressure solicitation, the height of the peaks was not constant since the compression load was not controlled. Under mechanical deformation due to gentle finger pressure a stable voltage was generated, compatible with the measured piezoelectric response.

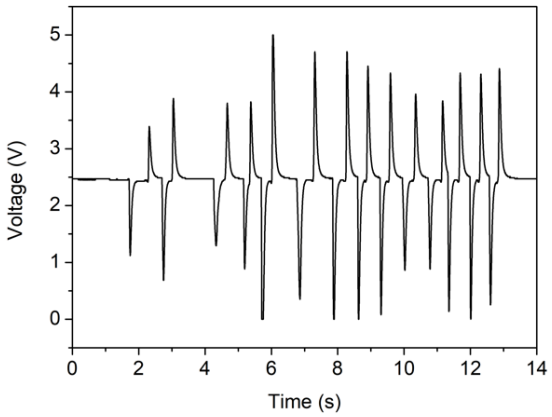

Figure 3. *Voltage generation throughout the piezoelectric PVDF membrane under pressure cycles.*

Despite the many efforts to elucidate the bone piezoelectric coefficients, the published data varies widely. Those attributed either to bone or tendons containing oriented collagen fibers usually differ by more than one order of magnitude [3,53–56]. Halperin et al. [57] studied the piezoelectric coefficients in dry and wet human bone and concluded that they vary in the range of 7 to 8 pC/N, in agreement with the results published by other authors [53,55]. Even though γ-PVDF electroactive response is lower than that of β-PVDF, the piezoelectric coefficient obtained is in the same order of magnitude as those reported by the aforementioned authors, indicating that γ-PVDF membranes are suitable candidates for future mesenchymal stem cell differentiation approaches.

PVDF thermal properties and degree of crystallinity were assessed by differential scanning calorimetry. The melting endotherm obtained at a heating range of 20 ºC/min is shown in Figure 2 (b). The melting peak indicating the melting temperature (T_m) of the PVDF membranes appears at 169.4 ± 1.2 ºC. Even though the γ polymorph shows a T_m around 8 ºC higher than α and β, as described by Gregorio [13], this polymorph is obtained from the isothermal crystallization at 166 ºC. Higher crystallization temperatures lead to higher crystallite sizes and raise the melting temperature. The PVDF membranes described here were obtained at 25 ºC, which resulted in a lower melting temperature, in agreement with the findings of Chang et al. [39,48], who manufactured PVDF membranes by the NIPS technique using different solvents and alcohols in the coagulation bath and obtained mostly γ-phase membranes with melting temperatures around 165-170 ºC.

The membrane's degree of crystallinity was obtained by applying Eq. (8). X_c is 65 ± 1 % for PVDF membranes, which confirms that liquid-liquid demixing is delayed by the non-solvents due to the reduced solvent-nonsolvent exchange rate. This delay allows crystallization to take place including nucleation and spherulite growth, producing membranes with a high percentage of crystalline phase within their structures.

3.2 ELRs deposition by the layer-by-layer technique

Surface fibronectin adsorption is a common technique when using PVDF as the cell culture support since its hydrophobicity hinders initial cell adhesion. However, the surface can be coated completely with other approaches, such as layer-by-layer ELRs deposition. Strong covalent bonds

are formed between the layers ensuring a permanent coating suitable for the tissue engineering field. This coating is considered cell-friendly because of ELRs' biocompatibility, as has been shown in previous works [58], and the copper-free click cross-linking between the layers. The click method involves the 1,3-dipolar cycloaddition of an azide and an especially active alkyne group, such as cyclooctyne (based on annular tension), allowing the reaction to take place without a catalyst [35] and applying atom economy.

An initial study was performed comprising the optimization and characterization of diverse coating conditions. The membrane activation time using the plasma treatment was first optimized and the RGD-N3 and RGD-CO solution concentration and the deposition order of the first layer was then studied. Once the optimal conditions were obtained the PVDF membranes were coated for cell culture tests by depositing two ELRs bilayers.

The PVDF membranes were activated by a simple, clean and effective plasma treatment method. The argon plasma flow (20 mL/min) was passed through a vacuum chamber (600 mTorr) and several time periods (1, 5, 20 and 30 minutes) were applied to the samples deposited inside. This step was controlled by measuring the contact angle of a drop of water on the PVDF membrane surface, as well as by FTIR-ATR. The activation step provides some oxidation of covalent bonds introducing a small number of hydroxyl groups at the surface that promote a small variation in the contact angle value observed before and after performing the activation. The small difference in the contact angle between non-activated (133 ± 1°) and activated membranes at different times (non-significant differences in contact angle values around 120°) slightly reduced hydrophobicity despite the plasma treatment.

FTIR-ATR of both pristine PVDF membrane and plasma activated one were performed after plasma treatment (see supplementary material, figure S1). The amount of hydroxyl groups introduced by argon plasma is not high enough to show substantial changes in the FTIR spectrum. However, in all the time periods tested, the activation was enough to immerse the samples in aqueous solutions for ELRs coating. The minimum activation time of 1 minute was chosen for the LbL process to avoid damaging the membranes.

Before membrane coating, the ELRs were chemically modified to carry azide and cyclooctyne functional groups, giving rise to RGD-N3 and RGD-CO, respectively. Both biopolymers were functionalized by modifying the ε-amine groups present in the lysines side chain, as described in Section 2.3.2. RGD-N3 and RGD-CO were characterized by ^{1}H-NMR spectroscopy, MALDI-ToF mass spectrometry and FTIR-ATR (see supplementary material).

The presence of twenty-four lysine residues distributed along the aminoacidic chain of the HRGD biopolymer allowed the amidation reaction of their amine groups with an N-succinimidyl carbonate derivative as a cyclooctyne carrier, giving rise to the RGD-CO biopolymer bearing cyclooctyne groups distributed along the ELR chain. A total of thirteen lysines were modified by 0.6 reagent equivalents, which yielded 90 % conversion. This conversion was determined by the MALDI-ToF and ^{1}H-NMR (in DMSO-d6) analysis, which enabled the quantification of the degree of lysine modification (supplementary material). The RGD-CO structure (Figure S2) was identified from the NMR signals and, above all, the integral value of H-N hydrogen from the newly formed carbamate allowed to quantify the number of amine groups modified. This lysine conversion value was consistent with the molecular weight increase recorded by the RGD-CO MALDI-ToF spectrometry (Figure S3).

Using 0.6 equivalents of an N-succinimidyl carbonate carrying azide group, HRGD was chemically modified in a similar amidation reaction to achieve RGD-N3. In this process, fourteen lysines were modified, giving a 97 % conversion rate. The number of lysines modified was calculated as explained above for RGD-CO (Figure S4 and S5 for ^{1}H-NMR and MALDI-ToF, respectively) but, in this case, the appearance of a new band at 2100 cm^{-1} in the FTIR-ATR spectrum confirmed the presence of azide groups in the RGD-N3 biopolymer chain (Figure S6).

After optimizing the time of PVDF membrane activation with plasma treatment and adequately modifying the biopolymers to achieve RGD-N3 and RGD-CO, the PVDF membrane coating process was optimized following the coating method described in Section 2.3.4. Layer-by-layer assays were performed at different RGD-CO and RGD-N3 solution concentrations (10 and 25 mg/mL) to study the influence of the ELRs solution concentration on the coating (Table 1). As the membranes were sequentially immersed in the ELRs solutions, the influence of the order of deposition of the first layer was also evaluated, obtaining four different types of coated membranes (a-d) (Table 1). The best coating was verified by the weight difference between uncoated and coated membranes per square cm as well as by water contact angle measurement (Table 1). As can be seen in Table 1, the largest weight increases were produced in membrane types a and b, which were first coated with RGD-N3, finishing the second bilayer with RGD-CO. The best of both coatings was obtained by the highest solution concentration of 25 mg/mL in membrane b. Coating verification by contact angle values showed lower hydrophobicity for membranes a and b than c and d, which is also consistent with the better coating of membranes a and b, and was optimal for membrane b, with the lowest contact angle value. These results are in agreement with the FTIR-ATR recorded for membranes a-d (Figure S7).

Table 1. *Parameters measured for different coatings on PVDF membranes to optimize coating protocol.*

Sample	First layer	Concentration (mg/mL)	ΔW/S (mg/cm^2)	Contact Angle (°)
a	RGD-N3	10	0.51	77 ± 3
b	RGD-N3	25	1.10	71 ± 1
c	RGD-CO	10	0.06	92 ± 6
d	RGD-CO	25	0.28	90 ± 6

Figure S7 gives the coated membrane spectrum showing the signals of the ELRs primarily characterized by absorption bands at 3300 and 1700 cm^{-1} of the N-H and C=O amidic bonds present in the main chain of ELRs, together with the characteristic absorption bands of the PVDF membranes in Figure 2, with bands ranging from 1300 to 500 cm^{-1}. Of the four types of FTIR-ATR membrane spectra, the largest absorption bands at 1700 cm^{-1} were those of membrane types a and b.

The PVDF membrane coating combination structure and morphology were also characterized by FESEM (Figure S8) and confirmed the results previously obtained by FTIR-ATR on the difference in weight and water contact angle. Sample b, coated with 25 mg/mL solutions of ELRs and RGD-N3 as the first layer deposited, was chosen to perform cell culture assays. Scheme 1 contains a description of the optimized chosen layer-by-layer protocol.

The characterization of the optimized layer-by-layer protocol is shown in Figure 4. Figure 4 (a) shows the FTIR-ATR spectra of the coated and non-coated membranes, where the ELRs peaks can be seen at about 1700 cm^{-1} and 3300 cm^{-1}, reconfirming the best LbL coating method. Images of

water contact angles before and after coating are shown in Figure 4 (b), confirming the reduced hydrophobicity accompanied by a smoother surface, as shown in Figure 1. Both the surface and cross-section FESEM images show the porous structure of the type b membranes. The cross-section image verifies correct membrane coating with a thin film evenly covering the surface.

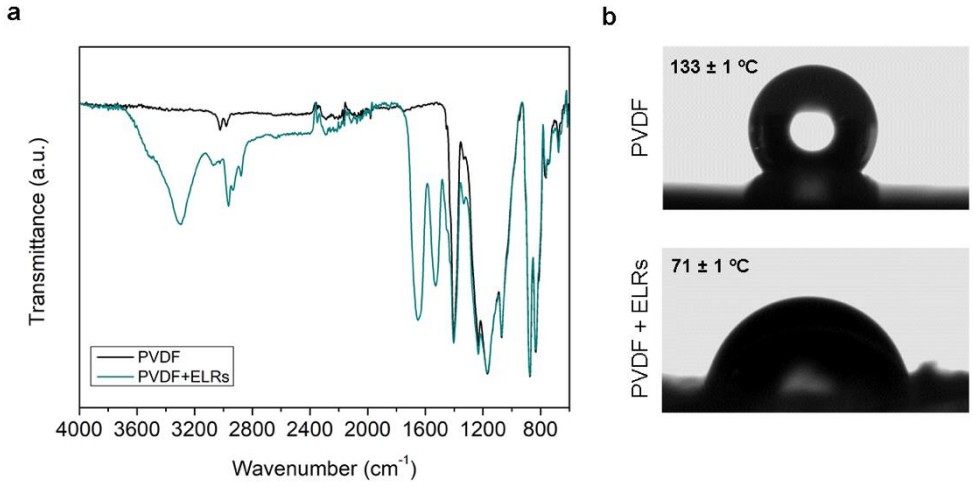

Figure 4*. (a) Comparison of FTIR-ATR spectra from type b coated membrane (blue line), and non-coated membrane (black line). (b) Images of the contact angles before (PVDF) and after (PVDF + ELRs) deposition of ELRs by the optimized protocol.*

3.3 pMSCs response to ELRs layer-by-layer coating

Porcine mesenchymal stem cells were used to test the initial cell adhesion and proliferation in PVDF membranes coated by LbL with ELRs or traditionally coated with adsorbed fibronectin. A glass slide coated with fibronectin was also used as the standard control. Nucleus-cytoskeleton staining at 24 h, 3 and 7 days was evaluated, as reported in Figure 5.

Figure 5 (a) shows that after 24 h cells had adhered in all the surfaces, showing an extended cytoskeleton in every condition. Despite this well-developed cytoskeleton, the differences in cell

number between conditions are significant. The PVDF membranes coated with fibronectin showed a negative fold change in cell proliferation, meaning that a lower number of cells than the initial cell seeding density attached on the surface. In the PVDF + ELRs condition, the cells had adhered and some had even proliferated after 24 h, as can be seen in Figure 5 (b), showing no significant differences with the glass slide control. However, the initial adhesion to PVDF was really poor and was not even able to retain the initial number of seeded cells.

The different proliferation rate can be seen after 7 days, when PVDF + ELRs and the glass slide have reached confluence, the fibronectin-coated PVDF has few cells and the proliferation rate is lower than in the other conditions.

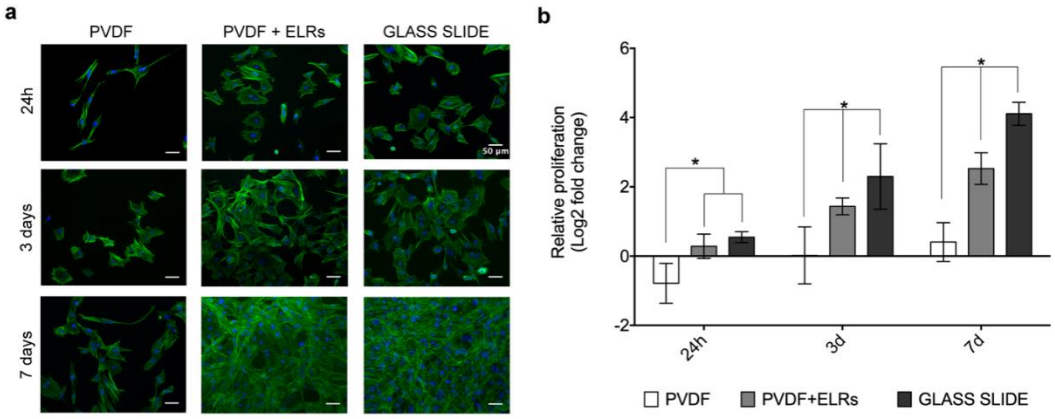

Figure 5. *(a) Representative images of actin (cytoskeleton-green) and DAPI (nucleus-blue) staining after 24 h, 3 and 7 days of culture for coated and uncoated PVDF membranes and glass slide control. Scale bar is 50 µm. (b) Cell count based on the analysis of 4 images taken from 3 replicates per condition at 24 h, 3 and 7 days from two independent assays. * p-value < 0.05*

Hydrophobicity is a key feature of PVDF, as demonstrated by the PVDF membrane contact angle before coating (133 ± 1 º). This effect is greatly increased by the membrane surface roughness due to spherulitic conformation.

This characteristic makes surface treatments an unavoidable approach for cell culture on PVDF. Since this polymer was first used in the tissue engineering field it has been traditionally coated with fibronectin [8,11,23]. In this study we found that fibronectin adsorption was not enough to promote initial cell adhesion to PVDF microporous membranes. This type of coating has been proven to be inefficient in spherulite-like PVDF membranes [24]. In a previous study we found that small changes in the degree of porosity in fibronectin-coated PVDF membranes can influence initial cell adhesion and proliferation in porcine bone marrow mesenchymal stem cells.

Contact angle is closely related to polymer wettability and also to surface roughness. Layer-by-layer deposition of elastin-like recombinamers reduced the water contact angle in PVDF membranes (71 ± 1 º), partially due to surface smoothing. The presence of RGD sequences in the ELRs and their deposition by LbL, which flattened the membrane surface, increased initial pMSCs adhesion in PVDF + ELRs membranes. The combination of both features makes this coating a suitable option for mesenchymal stem cell culture on porous PVDF membranes.

These findings lead the way to the use of PVDF membranes coated with elastin-like recombinamers containing RGD sequences in future MSCs differentiation approaches to the osteogenic lineage.

4. CONCLUSIONS

Non-solvent induced phase separation has proven to be a cost-effective and reliable technique for manufacturing PVDF membranes. The use of ethanol as non-solvent produced homogeneously porous membranes with more than 90 % γ-phase and up to 65 % overall crystalline content. Its electroactive potential was confirmed after poling by the contact method by measuring the d_{33} piezeoelectric coefficient, obtaining values within the bone piezoelectricity range. The membranes were coated with elastin-like recombinamers containing RGD sequences to improve their initial cell adhesion properties. ELRs were deposited by the layer-by-layer technique applying click cross-linking chemistry. After coating optimization, modified ELRs containing azide groups were selected for deposition as the first layer, followed by ELRs modified to contain cyclooctyne groups. Both layers reacted by interchain crosslinking via catalyst-free Hüisgen 1,3-dipolar cycloaddition, generating a stable bilayer. Two bilayers were deposited, reducing surface roughness and contact angle value. Cell adhesion and proliferation were tested on porcine bone marrow MSCs in a short-term culture (1 to 7 days). ELRs deposition by LbL was compared to traditional fibronectin adsorption and showed that cells preferred ELRs-coated surfaces for initial adhesion and proliferation. Fibronectin adsorption showed poor cell attachment and was not able to retain the initial number of seeded cells, while ELRs favoured adhesion and enhanced proliferation after 7 days. These findings open the door for the combination of electroactive PVDF membranes and synthetic peptides containing biofunctional sequences for mesenchymal stem cell culture and differentiation towards the osteogenic lineage.

SUPPLEMENTARY MATERIAL

Supplementary data associated with this article can be found in supplementary material: ^{1}H-NMR, MALDI-ToF and FTIR-ATR of RGD-CO and RGD-N3 for structure characterization of modified biopolymers together with FTIR-ATR of plasma-treated and PVDF-coated membranes and FESEM images of PVDF-coated and non-coated membranes for establishing optimal conditions.

ACKNOWLEDGMENTS

This work was supported by the Spanish State Research Agency (AEI) through Projects PID2019-106000RB-C21 / AEI / 10.13039/501100011033 and PID2019-106099RB-C43 / AEI / 10.13039/501100011033 (including FEDER funds). Maria Guillot-Ferriols received government funding for her doctoral thesis [grant number BES-2017-080398FPI]. The CIBER-BBN initiative is funded by the VI National R&D&I Plan 2008-2011, Iniciativa Ingenio 2010, Consolider Program. CIBER actions are financed by the Instituto de Salud Carlos III with assistance from the European Regional Development Fund. The authors are grateful for the funding from the Spanish Government (MAT2016-78903-R, RTI2018-096320-B-C22), Junta de Castilla y León (VA317P18), Interreg V España Portugal POCTEP (0624_2IQBIONEURO_6_E) and Centro en Red de Medicina Regenerativa y Terapia Celular de Castilla y León. This work was also supported by the Portuguese Foundation for Science and Technology (FCT) in the framework of the Strategic Funding UID/FIS/04650/2020. The authors thank FCT and FEDER funds (COMPETE 2020) under projects PTDC/BTM-MAT/28237/2017, PTDC/EMD-EMD/28159/2017 and PTDC/FIS-MAC/28157/2017. Carlos M. Costa is grateful to the FCT [grant number

FRH/BPD/112547/2015]. Financial support was also received from the Basque Government under the ELKARTEK, HAZITEK and PIBA (PIBA-2018-06) programs.

DATA AVAILABILITY

The raw data required to reproduce these findings are available from the corresponding authors upon request.

REFERENCES

[1] A.J. Lovinger, Annealing of Poly(vinylidene fluoride) and Formation of a Fifth Phase, Macromolecules. 15 (1982) 40–44. https://doi.org/10.1021/ma00229a008.

[2] P. Martins, A.C. Lopes, S. Lanceros-Mendez, Electroactive phases of poly(vinylidene fluoride): Determination, processing and applications, Prog. Polym. Sci. 39 (2014) 683–706. https://doi.org/10.1016/j.progpolymsci.2013.07.006.

[3] J. Jacob, N. More, K. Kalia, G. Kapusetti, Piezoelectric smart biomaterials for bone and cartilage tissue engineering, Inflamm. Regen. 38 (2018) 1–11. https://doi.org/10.1186/s41232-018-0059-8.

[4] E. Fukada, I. Yasuda, On the Piezoelectric Effect of Bone, J. Phys. Soc. Japan. 12 (1957) 1158–1162.

[5] A.C. Ahn, Alan J. Grodzinsky, Relevance of collagen piezoelectricity to “Wolff’s Law”: A critical review, 31 (2010) 733–741. https://doi.org/10.1016/j.medengphy.2009.02.006.RELEVANCE.

[6] C. Ribeiro, S. Moreira, V. Correia, V. Sencadas, J.G. Rocha, F.M. Gama, J.L. Gómez Ribelles, S. Lanceros-Méndez, Enhanced proliferation of pre-osteoblastic cells by dynamic piezoelectric stimulation, RSC Adv. 2 (2012) 11504. https://doi.org/10.1039/c2ra21841k.

[7] C. Ribeiro, D.M. Correia, S. Ribeiro, V. Sencadas, G. Botelho, S. Lanceros-Méndez, Piezoelectric poly(vinylidene fluoride) microstructure and poling state in active tissue engineering, Eng. Life Sci. 15 (2015) 351–356. https://doi.org/10.1002/elsc.201400144.

[8] R. Sobreiro-Almeida, M. Tamaño-Machiavello, E. Carvalho, L. Cordón, S. Doria, L. Senent, D. Correia, C. Ribeiro, S. Lanceros-Méndez, R. Sabater i Serra, J. Gomez Ribelles, A. Sempere, Human Mesenchymal Stem Cells Growth and Osteogenic Differentiation on Piezoelectric Poly(vinylidene fluoride) Microsphere Substrates, Int. J. Mol. Sci. 18 (2017) 2391. https://doi.org/10.3390/ijms18112391.

[9] N. Castro, S. Ribeiro, M.M. Fernandes, C. Ribeiro, V. Cardoso, V. Correia, R. Minguez, S. Lanceros-Mendez, Physically Active Bioreactors for Tissue Engineering Applications, Adv. Biosyst. 4 (2020) 1–29. https://doi.org/10.1002/adbi.202000125.

[10] N. Castro, M.M. Fernandes, C. Ribeiro, V. Correia, R. Minguez, S. Lanceros-Mendez, Magnetic Bioreactor for Magneto-, Mechano- and Electroactive Tissue Engineering Strategies, Sensors. 20 (2020) 3340. https://doi.org/doi:10.3390/s20123340.

[11] C. Ribeiro, J. Pärssinen, V. Sencadas, V. Correia, S. Miettinen, V.P. Hytönen, S. Lanceros-Méndez, Dynamic piezoelectric stimulation enhances osteogenic differentiation of human adipose stem cells, J. Biomed. Mater. Res. - Part A. 103 (2015) 2172–2175. https://doi.org/10.1002/jbm.a.35368.

[12] S. Ribeiro, C. Ribeiro, E.O. Carvalho, C.R. Tubio, N. Castro, N. Pereira, V. Correia, A.C. Gomes, S. Lanceros-Méndez, Magnetically Activated Electroactive Microenvironments for Skeletal Muscle Tissue Regeneration, ACS Appl. Bio Mater. 3 (2020) 4239–4252. https://doi.org/10.1021/acsabm.0c00315.

[13] R. Gregorio, Determination of the α, β, and γ crystalline phases of poly(vinylidene fluoride) films prepared at different conditions, J. Appl. Polym. Sci. 100 (2006) 3272–3279. https://doi.org/10.1002/app.23137.

[14] V. Sencadas, R. Gregorio, S. Lanceros-Méndez, α to β phase transformation and microestructural changes of PVDF films induced by uniaxial stretch, J. Macromol. Sci. Part B Phys. 48 (2009) 514–525. https://doi.org/10.1080/00222340902837527.

[15] M. Pagliero, A. Bottino, A. Comite, C. Costa, Novel hydrophobic PVDF membranes prepared by nonsolvent induced phase separation for membrane distillation, J. Memb. Sci. 596 (2020). https://doi.org/10.1016/j.memsci.2019.117575.

[16] T. Boccaccio, A. Bottino, G. Capannelli, P. Piaggio, Characterization of PVDF membranes by vibrational spectroscopy, J. Memb. Sci. 210 (2002) 315–329. https://doi.org/10.1016/S0376-7388(02)00407-6.

[17] C. Ribeiro, C.M. Costa, D.M. Correia, J. Nunes-Pereira, J. Oliveira, P. Martins, R. Gonçalves, V.F. Cardoso, S. Lanceros-Méndez, Electroactive poly(vinylidene fluoride)-based structures for advanced applications, Nat. Protoc. 13 (2018) 681–704. https://doi.org/10.1038/nprot.2017.157.

[18] X. Wang, L. Zhang, D. Sun, Q. An, H. Chen, Formation mechanism and crystallization of

poly(vinylidene fluoride) membrane via immersion precipitation method, Desalination. 236 (2009) 170–178. https://doi.org/10.1016/j.desal.2007.10.064.

[19] L.P. Cheng, Effect of temperature on the formation of microporous PVDF membranes by precipitation from 1-Octanol/DMF/PVDF and water/ DMF/PVDF systems, Macromolecules. 32 (1999) 6668–6674. https://doi.org/10.1021/ma990418l.

[20] F. Liu, N.A. Hashim, Y. Liu, M.R.M. Abed, K. Li, Progress in the production and modification of PVDF membranes, J. Memb. Sci. 375 (2011) 1–27. https://doi.org/10.1016/j.memsci.2011.03.014.

[21] M. Guillot-Ferriols, J.C. Rodríguez-Hernández, D.M. Correia, S.A.C. Carabineiro, S. Lanceros-Méndez, J.L. Gómez Ribelles, G. Gallego Ferrer, Poly(vinylidene) fluoride membranes coated by heparin / collagen layer-by-layer, smart biomimetic approaches for mesenchymal stem cell culture, Mater. Sci. Eng. C. 117 (2020) 111281. https://doi.org/10.1016/j.msec.2020.111281.

[22] K. Webb, V. Hlady, P.A. Tresco, Relative importance of surface wettability and charged functional groups on NIH 3T3 fibroblast attachment, spreading, and cytoskeletal organization, J. Biomed. Mater. Res. 41 (1998) 422–430. https://doi.org/10.1002/(SICI)1097-4636(19980905)41:3<422::AID-JBM12>3.0.CO;2-K.

[23] C. Ribeiro, J.A. Panadero, V. Sencadas, S. Lanceros-M??ndez, M.N. Tama??o, D. Moratal, M. Salmer??n-S??nchez, J.L. G??mez Ribelles, Fibronectin adsorption and cell response on electroactive poly(vinylidene fluoride) films, Biomed. Mater. 7 (2012). https://doi.org/10.1088/1748-6041/7/3/035004.

[24] R.M. Morales-Román, M. Guillot-Ferriols, L. Roig-Pérez, S. Lanceros-Mendez, G. Gallego-Ferrer, J.L. Gómez Ribelles, Freeze-extraction microporous electroactive supports for cell culture, Eur. Polym. J. 119 (2019) 531–540. https://doi.org/10.1016/j.eurpolymj.2019.07.011.

[25] J.C. Rodríguez-Cabello, L. Martín, M. Alonso, F.J. Arias, A.M. Testera, "Recombinamers" as advanced materials for the post-oil age, Polymer (Guildf). 50 (2009) 5159–5169. https://doi.org/10.1016/j.polymer.2009.08.032.

[26] A. Girotti, J. Reguera, J.C. Rodríguez-Cabello, F.J. Arias, M. Alonso, A.M. Testera, Design and bioproduction of a recombinant multi(bio)functional elastin-like protein polymer containing cell adhesion sequences for tissue engineering purposes, J. Mater. Sci. Mater. Med. 15 (2004) 479–484. https://doi.org/10.1023/B:JMSM.0000021124.58688.7a.

[27] M.C. Berg, S.Y. Yang, P.T. Hammond, M.F. Rubner, Controlling Mammalian Cell Interactions on Patterned Polyelectrolyte Multilayer Surfaces, Langmuir. 20 (2004) 1362–1368. https://doi.org/10.1021/la0355489.

[28] E. Ruoslahti, RGD and Other Recognition Sequences for Integrins, Annu. Rev. Cell Dev. Biol. 12 (1996) 697–715. https://doi.org/10.1146/annurev.cellbio.12.1.697.

[29] A. Nicol, D. Channe Gowda, D.W. Urry, Cell adhesion and growth on synthetic elastomeric matrices containing ARG-GLY–ASP–SER–3, J. Biomed. Mater. Res. 26 (1992) 393–413. https://doi.org/10.1002/jbm.820260309.

[30] R.R. Costa, C.A. Custódio, A.M. Testera, F.J. Arias, J.C. Rodríguez-Cabello, N.M. Alves, J.F. Mano, Stimuli-responsive thin coatings using elastin-like polymers for biomedical

applications, Adv. Funct. Mater. 19 (2009) 3210–3218. https://doi.org/10.1002/adfm.200900568.

[31] Z. Qu, J. Yan, B. Li, J. Zhuang, Y. Huang, Improving bone marrow stromal cell attachment on chitosan/hydroxyapatite scaffolds by an immobilized RGD peptide, Biomed. Mater. 5 (2010). https://doi.org/10.1088/1748-6041/5/6/065001.

[32] F. Yang, C.G. Williams, D.A. Wang, H. Lee, P.N. Manson, J. Elisseeff, The effect of incorporating RGD adhesive peptide in polyethylene glycol diacrylate hydrogel on osteogenesis of bone marrow stromal cells, Biomaterials. 26 (2005) 5991–5998. https://doi.org/10.1016/j.biomaterials.2005.03.018.

[33] H. Shin, J.S. Temenoff, G.C. Bowden, K. Zygourakis, M.C. Farach-Carson, M.J. Yaszemski, A.G. Mikos, Osteogenic differentiation of rat bone marrow stromal cells cultured on Arg-Gly-Asp modified hydrogels without dexamethasone and β-glycerol phosphate, Biomaterials. 26 (2005) 3645–3654. https://doi.org/10.1016/j.biomaterials.2004.09.050.

[34] J.M. Anderson, J.B. Vines, J.L. Patterson, H. Chen, A. Javed, H.-W. Jun, Osteogenic differentiation of human mesenchymal stem cells synergistically enhanced by biomimetic peptide amphiphiles combined with conditioned medium, Acta Biomater. 7 (2012) 675–682. https://doi.org/10.1016/j.actbio.2010.08.016.Osteogenic.

[35] I. González De Torre, M. Santos, L. Quintanilla, A. Testera, M. Alonso, J.C. Rodríguez Cabello, Elastin-like recombinamer catalyst-free click gels: Characterization of poroelastic and intrinsic viscoelastic properties, Acta Biomater. 10 (2014) 2495–2505.

https://doi.org/10.1016/j.actbio.2014.02.006.

[36] D.L. Nettles, A. Chilkoti, L.A. Setton, Applications of elastin-like polypeptides in tissue engineering, Adv. Drug Deliv. Rev. 62 (2010) 1479–1485. https://doi.org/10.1016/j.addr.2010.04.002.

[37] M.P. Sousa, I. Gonzalez de Torre, M.B. Oliveira, J.C. Rodríguez-Cabello, J.F. Mano, Biomimetic click assembled multilayer coatings exhibiting responsive properties, Mater. Today Chem. 4 (2017) 150–163. https://doi.org/10.1016/j.mtchem.2017.04.001.

[38] M. Benz, W.B. Euler, Determination of the crystalline phases of poly(vinylidene fluoride) under different preparation conditions using differential scanning calorimetry and infrared spectroscopy, J. Appl. Polym. Sci. 89 (2003) 1093–1100. https://doi.org/10.1002/app.12267.

[39] H.H. Chang, L.K. Chang, C.D. Yang, D.J. Lin, L.P. Cheng, Effect of polar rotation on the formation of porous poly(vinylidene fluoride) membranes by immersion precipitation in an alcohol bath, J. Memb. Sci. 513 (2016) 186–196. https://doi.org/10.1016/j.memsci.2016.04.052.

[40] A.C. Lopes, C.M. Costa, C.J. Tavares, I.C. Neves, S. Lanceros-Mendez, Nucleation of the electroactive γ phase and enhancement of the optical transparency in low filler content poly(vinylidene)/clay nanocomposites, J. Phys. Chem. C. 115 (2011) 18076–18082. https://doi.org/10.1021/jp204513w.

[41] K. Nakagawa, Y. Ishida, Annealing effects in poly(vinylidene fluoride) as revealed by specific volume measurements, differential scanning calorimetry, and electron microscopy,

J. Polym. Sci. Part A-2 Polym. Phys. 11 (1973) 2153–2171. https://doi.org/10.1002/pol.1973.180111107.

[42] G. Pinedo-Martín, M. Santos, A.M. Testera, M. Alonso, J.C. Rodríguez-Cabello, The effect of NaCl on the self-assembly of elastin-like block co-recombinamers: Tuning the size of micelles and vesicles, Polymer (Guildf). 55 (2014) 5314–5321. https://doi.org/10.1016/j.polymer.2014.08.053.

[43] D.E. Meyer, A. Chilkoti, Purification of recombinant proteins by fusion with thermally-responsive polypeptides, Nat. Biotechnol. 17 (1999) 1112–1115. https://doi.org/10.1038/15100.

[44] A. Girotti, D. Orbanic, A. Ibáñez-Fonseca, C. Gonzalez-Obeso, J.C. Rodríguez-Cabello, Recombinant Technology in the Development of Materials and Systems for Soft-Tissue Repair, Adv. Healthc. Mater. 4 (2015) 2423–2455. https://doi.org/10.1002/adhm.201500152.

[45] J.T. Jung, J.F. Kim, H.H. Wang, E. di Nicolo, E. Drioli, Y.M. Lee, Understanding the non-solvent induced phase separation (NIPS) effect during the fabrication of microporous PVDF membranes via thermally induced phase separation (TIPS), J. Memb. Sci. 514 (2016) 250–263. https://doi.org/10.1016/j.memsci.2016.04.069.

[46] D.J. Lin, K. Beltsios, T.H. Young, Y.S. Jeng, L.P. Cheng, Strong effect of precursor preparation on the morphology of semicrystalline phase inversion poly(vinylidene fluoride) membranes, J. Memb. Sci. 274 (2006) 64–72. https://doi.org/10.1016/j.memsci.2005.07.043.

[47] D.J. Lin, K. Beltsios, C.L. Chang, L.P. Cheng, Fine structure and formation mechanism of particulate phase-inversion poly(vinylidene fluoride) membranes, J. Polym. Sci. Part B Polym. Phys. 41 (2003) 1578–1588. https://doi.org/10.1002/polb.10513.

[48] H.H. Chang, L.K. Chang, C.D. Yang, D.J. Lin, L.P. Cheng, Effect of solvent on the dipole rotation of poly(vinylidene fluoride) during porous membrane formation by precipitation in alcohol baths, Polymer (Guildf). 115 (2017) 164–175. https://doi.org/10.1016/j.polymer.2017.03.044.

[49] K.M. Kim, W.S. Jeon, N.G. Park, K.S. Ryu, S.H. Chang, Effect of evaporation temperature on the crystalline properties of solution-cast films of poly(vinylidene fluoride)s, Korean J. Chem. Eng. 20 (2003) 934–941. https://doi.org/10.1007/BF02697302.

[50] E. Lizundia, A. Reizabal, C.M. Costa, A. Maceiras, S. Lanceros-Méndez, Electroactive γ-Phase, Enhanced Thermal and Mechanical Properties and High Ionic Conductivity Response of Poly (Vinylidene Fluoride)/Cellulose Nanocrystal, Materials (Basel). 13 (2020) 743. https://doi.org/doi:10.3390/ma13030743.

[51] A. Salimi, A.A. Yousefi, Conformational changes and phase transformation mechanisms in PVDF solution-cast films, J. Polym. Sci. Part B Polym. Phys. 42 (2004) 3487–3495. https://doi.org/10.1002/polb.20223.

[52] S. Gonçalves, J. Serrado-Nunes, J. Oliveira, N. Pereira, L. Hilliou, C.M. Costa, S. Lanceros-Méndez, Environmentally Friendly Printable Piezoelectric Inks and Their Application in the Development of All-Printed Touch Screens, ACS Appl. Electron. Mater. 1 (2019) 1678–1687. https://doi.org/10.1021/acsaelm.9b00363.

[53] A.R. Liboff, M. Furst, Pyroelectric Effect in Collagenous Structures, Ann. N. Y. Acad. Sci. 238 (1974) 26–35. https://doi.org/10.1111/j.1749-6632.1974.tb26777.x.

[54] E. Fukada, Mechnical deformation and electrical polarization in biological substances., Biorheology. 5 (1968) 199–208. https://doi.org/10.3233/BIR-1968-5302.

[55] E. Fukada, I. Yasuda, Piezoelectric Effects in Collagen, Japanese J. Appl. Physics, Part 1 Regul. Pap. Short Notes Rev. Pap. 3 (1964) 502B. https://doi.org/10.1143/jjap.3.502b.

[56] S.B. Lang, Piezoelectricity, pyroelectricity and ferroelectricity in biomaterials: Speculation on their biological significance, IEEE Trans. Dielectr. Electr. Insul. 7 (2000) 466–473. https://doi.org/10.1109/94.868063.

[57] C. Halperin, S. Mutchnik, A. Agronin, M. Molotskii, P. Urenski, M. Salai, G. Rosenman, Piezoelectric effect in human bones studied in nanometer scale, Nano Lett. 4 (2004) 1253–1256. https://doi.org/10.1021/nl049453i.

[58] I.G. De Torre, F. Wolf, M. Santos, L. Rongen, M. Alonso, S. Jockenhoevel, J. C.Rodríguez-Cabello, P. Mela, Elastin-like recombinamer-covered stents: Towards a fully biocompatible and non-thrombogenic device for cardiovascular diseases, Acta Biomater. 12 (2015) 146–155. https://doi.org/10.1016/j.actbio.2014.10.029.